rhoCentralRfFoam: An OpenFOAM solver for high speed chemically active flows –Simulation of planar detonations–

Gutiérrez Marcantoni, L. F[a,b,*], Tamagno, J.[a], Elaskar, S.[a,b]

[a] *Facultad de Ciencias Exactas, Físicas y Naturales, Universidad Nacional de Córdoba, Córdoba, Argentina*
[b] *Consejo Nacional de Investigaciones Científicas y Técnicas, (CONICET)*

Abstract

A new solver developed within the framework of OpenFOAM 2.3.0, called `rhoCentralRfFoam` which can be interpreted like an evolution of `rhoCentralFoam`, is presented. Its use, performing numerical simulations on initiation and propagation of planar detonation waves in combustible mixtures $H_2 - Air$ and $H_2 - O_2 - Ar$, is described. Unsteady one dimensional (1D) Euler equations coupled with sources to take into account chemical activity, are numerically solved using the Kurganov, Noelle and Petrova second order scheme in a domain discretized with finite volumes. The computational code can work with any number of species and its corresponding reactions, but here it was tested with 13 chemically active species (one species inert), and 33 elementary reactions. A gaseous igniter which acts like a shock-tube driver, and powerful enough to generate a strong shock capable of triggering exothermic chemical reactions in fuel mixtures, is used to start planar detonations. The following main aspects of planar detonations are here, treated: induction time of combustible mixtures cited above and required mesh resolutions; convergence of overdriven detonations to Chapman-Jouguet states; detonation structure (ZND model); and the use of reflected shocks to determine induction times experimentally. The `rhoCentralRfFoam` code was verified comparing numerical results and it was validated, through analytical results and experimental data.

Keywords: Kurganov schemes, OpenFOAM®, detonation, induction time

1. Introduction

There are two extreme modes of combustion in any gaseous fuel mixture: deflagration and detonation. In deflagrations the flame propagation velocities are of the order of a few meters per second and the corresponding pressure increase is small. They are governed by diffusion of heat and mass from reacting zone to unburned mixture. On the other hand, detonation waves can reach speeds up to $2000\,ms^{-1}$ and pressures 20 times higher than the initial value of the unburned mixture. Detonations are mainly triggered by adiabatic shock compression that increase temperature and pressure of the unburned mixture above ignition conditions [1]. In this work, only detonations in homogeneous combustible mixtures of $H_2 - Air$ and $H_2 - O_2$ diluted with argon, are considered.

*Corresponding author
Email address:
`luisfelipegutierrezmarcantoni@conicet.gov.ar` (Gutiérrez Marcantoni, L. F)

The classical Chapman-Jouguet (CJ) theory, seeks the unique solution of one dimensional conservation equations across detonation fronts in which the flow behind the wave, is sonic (CJ condition). It includes thermodynamic calculations for each detonation parameter (i.e. pressure, temperature and density ratios across the wave and mixture composition), the detonation velocity, and composition of the burned mixture. In the CJ theory it is assumed that chemical reactions take place instantaneously inside the shock (i.e, the reaction zone length would shrink to zero), nevertheless detonation static parameters obtained by the classical CJ approach are in good agreement with experimental observations [1, 2, 3]. But, parameters like the initiation energy, detonability limits, the thickness of the reaction zone, requires the knowledge of the wave structure itself, and hence of the chemical kinetic process expressed through finite reaction rates.

In this context, a study on starting and propagating planar unconfined detonations, based on solving unsteady flow equations coupled with finite rate chemical processes, has been carried out. To start a planar detonation, and to keep it always like that, a planar igniter must be used. Such igniter has been conceived as a region adjacent to detonation system closed end, filled with a high temperature and pressure gas, either with combustion products or an inert gas (like helium). Then, the igniter is like a shock tube driver and uses its energy to drive through a combustible mixture a blast (or strong shock) capable of starting the necessary exothermic chemical reactions to induce a sustainable detonation. A detonation can be analyzed assuming that it behaves like a traveling strong shock, therefore existing fluid dynamics methods may be extended and adapted to generate suitable numerical codes for detonating processes simulations [4, 5].

In the last years OpenFOAM® [6, 7, 8] has become in a very popular finite volume library for solving a broad range of computational fluid dynamics problems. It has been tested in many fields (i.e, incompressible flow applications [9, 10, 11, 12, 13, 14], multiphase flows [15, 16, 17, 18], low speed reactive flow problems [19, 20, 21, 22], non-Newtonian fluids [23, 24], high speed not reactive flows [25, 26, 27, 28, 29], among others). In this work, OpenFOAM® libraries were selected to build a new solver `rhoCentralRfFoam` (Rf stands for *Reacciones Finitas*; Spanish translation for Finite Reactions), to be used in simulations of high speed reactive flows with detailed chemistry [30, 31, 32].

Although the OpenFOAM® framework has been used to simulate high speed reactive flows, the approach adopted here (i.e, studying planar detonations with Kurganov central schemes and detailed chemistry) has not been largely employed to simulate detonation processes. The work of Bansal et al. presents a study of atmospheric reentry problem with coupling of radiative effects, showing that OpenFOAM® can be an appropriate tool for studying high speed reactive flow [33]. Recently Casseau et al., develop the solvers `hyFoam` and `hyFoam2` for hypersonic high temperature dissociating gas mixtures [34, 35, 35]. `hyFoam` and `hyFoam2` used respectively, one temperature and two temperature approaches. The work of Ettner et al. [36] performed in the context of a PISO-HLLC hybrid method, describes simulations with OpenFOAM® of deflagration-detonation transitions (ddt). The chemical kinetic process is modeled extracting interpolated induction time values from an external data base built in terms of pressure, temperature and mixture fraction of hydrogen

atoms, that is, without resolving the micro-structure of the flow in a true CFD grid. Furthermore, the detonation onset is modeled by adding artificial sources. In the present work a detailed chemical kinetic model is solved at each cell and each simulation step. The combustion process is taken into account by transport equations for species, appropriate source terms for its production/consumption and the heat released by fuel burning.

In this work convective terms are evaluated through an adaptation of the second order central-upwind numerical scheme of Kurganov, Noelle and Petrova (NKP) [37], previously introduced for non reactive flow simulations on the solver known as `rhoCentralFoam` [25]. The chemical process is taken into account in a similar way as used in the low speed combustion solver `reactingFoam`. The new solver can be seen like a sort of merging the two mentioned solvers. `rhoCentralRfFoam` will be tested on computing detonation propagation processes. It is important to note that in despite of 1D applications shown here, the `rhoCentralRfFoam` solver can also be used to simulate 2D and 3D dimensional detonations. Simulations of 2D and 3D configurations will be addressed in future works.

Detonations are time dependent problems (unsteady fluid dynamics and finite chemical rates), therefore, the accumulation of errors from numerical damping must be avoided [38]. To avoid such errors, in this work an explicit fractional step technique (or time splitting approach) which decouple the fluid transport process from the reactive one, is applied [39]. This leads to an ODE system associated with the chemical kinetic model, but this ODE system is stiff, and to be solved a proper algorithm is needed. Here the semi-implicit Bader and Deuflhard [40] version of the Bulirsh-Stöer explicit mid-point rule is employed (SIBS algorithm from OpenFOAM® libraries) [41].

2. Reactive Euler equations

The flow is described by the inviscid, non-conducting reactive Euler equations [42]:

$$\frac{\partial \mathbf{u}}{\partial t} + \frac{\partial \mathbf{F}}{\partial x_i} = \mathbf{Q} \tag{1}$$

where $\mathbf{u}$ are the conservative variables, $\mathbf{F}$ the corresponding fluxes and $\mathbf{Q}$ the source terms. Then

$$\mathbf{u} = [\rho, (\rho\mathbf{U}), (\rho E), (\rho Y_k)]^{\mathrm{T}} \tag{2}$$

$$\mathbf{F} = [\rho\mathbf{U}, (\rho\mathbf{U}\mathbf{U} + \mathrm{p}), (\rho E\mathbf{U} + \mathbf{U}\mathrm{p}), (\rho Y_k\mathbf{U})]^{\mathrm{T}} \tag{3}$$

$$\mathbf{Q} = [0, (\mathbf{0}), (\dot{\omega}_{\mathbf{T}}), (\dot{\omega}_{\mathbf{k}})]^{\mathrm{T}} \tag{4}$$

Given the mass fractions condition $\sum^{N} Y_k = 1$, for 1D simulations a set of $N + 2$ transport equations for each control volume is required. A non chemical total energy (E) is defined as [43]:

$$E = h_s - p\rho^{-1} + \frac{1}{2}\|\mathbf{U}\|^2 \tag{5}$$

and the sensible enthalpy (h_s) is related to temperature by

$$h_s = \int_{T_0}^{T} c_p \, dT \tag{6}$$

The implicit Eq. (6) for temperature is solved by using a Newton-Rhapson iterative technique. Pressure constant heat capacity (c_p) is a temperature and species mass fractions function, therefore this functional dependence is modeled by computing c_p from

$$c_p = \sum_{k=1}^{N} c_{p_k} Y_k \tag{7a}$$

$$c_{p_k} = c_{p_k}^{\mathrm{o}} \mathrm{W_k}^{-1} \tag{7b}$$

Species molar constant pressure heat capacities ($c_{p_k}^{\circ}$) are obtained using the JANAF polynomials [44], thus

$$c_{p_k}^{\circ} = \sum_{j=0}^{6} a_j T^j \tag{8}$$

The heat capacity ratio (γ) is calculated by

$$\gamma = \frac{c_p}{c_p - R} \tag{9}$$

where $R = R_u \sum^N Y_k W_k^{-1}$ (with R_u the universal gas constant). Thermal state equation for a mixture of N ideal gases can be written [43]

$$p = \sum_{i}^{N} p_k \tag{10}$$

$$= T\rho R_u \sum_{k=1}^{N} Y_k W_k^{-1} \tag{11}$$

The energy equation source term is given by [43]

$$\dot{\omega}_{\mathrm{T}} = \sum_{k=1}^{N} \dot{\omega}_{\mathrm{k}} \Delta h_{f,k}^{\circ} \tag{12}$$

where $\dot{\omega}_{\mathrm{k}}$ are the production/consumption rates of the species k and $\Delta h_{f,k}^{\circ}$ its formation (chemical) enthalpy. The production/consumption rate of all species are related to the chemical kinetic model, then the mass rate of any species k by reaction i is

$$\dot{\omega}_{k,i} = [\dot{C}_{\mathrm{k},i}] W_{\mathrm{k}} \tag{13}$$

W_k is the molecular weight of species k and $[\dot{C}_{k,i}]$ its molar rate.

3. Chemical source terms

To compute source terms in species and energy equations, appropriate chemical kinetics models are needed. Chemical models describe the M elementary reactions and N species interaction which in compact form can be written [43]

$$\sum_{k=1}^{N} \nu_{ki}^{'}[C_k] \overset{k_i^f}{\longrightarrow} \sum_{k=1}^{N} \nu_{ki}^{''}[C_k] \tag{14}$$

$$\sum_{k=1}^{N} \nu_{ki}^{'}[C_k] \overset{k_i^b}{\longleftarrow} \sum_{k=1}^{N} \nu_{ki}^{''}[C_k] \tag{15}$$

Here $\nu_{ki}^{'}$ and $\nu_{ki}^{''}$ are the reactants and products stoichiometric coefficients, k_i^f and k_i^b are the forward and backward rates constants and $[C_k]$ the molar concentration of the species k. The system is represented by a matrix of stoichiometric coefficients with dimensions $N \times M$ in which, rows represents the species and columns reactions. Then, each rate of the species j related to reaction i can be written [43]

$$\dot{\omega}_{k,i}^{\circ} = (\nu_{\mathrm{ki}}^{''} - \nu_{\mathrm{ki}}^{'}) \sum_{k=1}^{N} (\alpha_k [C_k]) \left[k_i^f \prod_{k=1}^{N} [C_k]^{\nu_{\mathrm{ki}}^{'}} - k_i^b \prod_{k=1}^{N} [C_k]^{\nu_{\mathrm{ki}}^{''}} \right] \tag{16}$$

where α_k expresses the third body efficiency of species k. The rate of species k by all involved reactions written on a mass basis is:

$$\dot{\omega}_{\mathrm{k}} = W_k \sum_{i=1}^{M} \dot{\omega}_{\mathrm{k,i}}^{\circ} \tag{17}$$

being W_k the molecular mass. The chemistry modeling involves solving N stiff ODEs in each control volume and time step. This ODE system involves an equation for each species with its corresponding forward and backward contributions. The forward reaction rates constants are defined by using the Arrhenius law [45, 43]:

$$k_i^f = A T^b \exp\left(\frac{E_a}{RT}\right) \tag{18}$$

where A is the pre-exponential factor, b the temperature exponent, and E_a the activation energy. The pressure dependence for reactions (i.e, R_4,R_5,R_6,R_7, and R_{21}) is considered through Lindemann form [45]:

$$k^f = k_{\infty} \left(\frac{P_r}{1 + P_r}\right) F \tag{19}$$

being P_r the so-called reduced pressure related to the mixture $[C_M]$ concentration by [43]

$$P_r = \frac{k_0[C_M]}{k_\infty} \tag{20}$$

k_∞[1] is the high-pressure limit rate constant and k_0 the low-pressure limit rate constant (Low keyword in Table. A.3). For the Lindemann approach F function in Eq. 19 is taken as unity (R_4, R_5, R_6, R_7). In the method proposed by Troe the function F is written [46]

$$\log F = \left\{1 + \left[\frac{\log P_r + c}{n - d\,(\log P_r + c)}\right]^2\right\}^{-1} \log F_{cent} \tag{21}$$

where

$$c = -0.4 - 0.67\log(F_{cent})$$

$$n = 0.75 - 1.27\log(F_{cent})$$

$$F_{cent} = (1-a)\exp\frac{-T}{T^{***}} + a\exp\frac{-T}{T^{*}} + \exp\frac{-T^{**}}{T}$$

The a, T^{***}, T^{*} and T^{**} parameters are specified as inputs on the typical format of CHEMKIN (R_{21}, keyword Troe in Table. A.3). The backward rate constants are computed by [43]:

$$k_i^b = k_i^f K_{C,i}^{-1} \tag{22}$$

where $K_{C,i}$ are the equilibrium constants, determined by the following relation [43]

$$K_{C,i} = \prod_{k=1}^{N} \overline{C}_k^{(\nu''_{ki} - \nu'_{ki})} \tag{23}$$

note that $\overline{C}_k$ is for species k, the molar concentration at thermodynamic equilibrium.

4. Numerical procedures

The governing equations with the chemical kinetic model contributions are solved by using a fractional step method (also known as time splitting approach). This technique decouple the transport process from the reactive one [39]. The ODE system associated with the kinetic model is solved by utilizing the semi-implicit Bulirsch-Stöer method (SIBS) [41, 40].

The finite volume discretization scheme is formulated taking advantage of the data structure provided by the OpenFOAM® platform. Discrete convective terms are evaluated with the second order central upwind scheme introduced by Kurganov, Noelle and Petrova [37] and tested for non-reactive flows in [25, 27].

4.1. Fractional step approach

It can be argued that the major advantage of implicit methods is that the time step Δt is not conditioned (at least theoretically) by stability considerations. However, their principal disadvantage is the large system of nonlinear equations solution at each time step, which makes implicit methods excessively expensive even for 1D reacting flow simulations. Also, it has been demonstrated that the use of large time steps in a fully implicit approach, increases the numerical damping making the obtained numerical results less accurate in time [38].

Fractional step approach is based on the time-operator splitting introduced in [39]. The overall reactive flow equations are split into the subproblems[2]:

$$\frac{\partial}{\partial t}(\psi) = S(\psi, t) \quad \text{CI: } \psi^{n-1} \xrightarrow{\Delta\tau^c} \widehat{\psi}^{\,n} \tag{24a}$$

$$\frac{\partial}{\partial t}(\psi) + \mathcal{L}(\psi) = S(\widehat{\psi}, t) \quad \text{CI: } \widehat{\psi}^{\,n} \xrightarrow{\Delta t} \psi^{\,n} \tag{24b}$$

To integrate the ODE system of Eq. (24a) the SIBS method from OpenFOAM® library is employed. To compute the solution at t^n, the integration chemical time

[1] Note that k_∞ in Eq.19 is given by Eq. 18, assuming that the rate constant is computed at the hight pressure limit

[2] Note that $\widehat{\psi}^{\,n}$ is the first fractional step problem solution, information then used to evaluate the source terms for the second stage.

step $\Delta\tau^c$ is divided in n sub steps that are determined by the modified midpoint technique which are then extrapolated by the Aitken-Neville algorithm to obtain new concentration values. Once the concentrations are actualized, source terms in species and energy equations are computed, and then the fluid-dynamic system is evolved to $t + \Delta t$ [40].

4.2. Finite volume formulation

Transport equations for mass, momentum, energy and species mass fractions are discretized by the finite volume method. For any arbitrary tensorial quantity $\boldsymbol{\psi}$, the integral form of a generic unsteady convection-reaction equation can be written [47]

$$\frac{\partial}{\partial t}\int_V \rho\boldsymbol{\psi}\mathrm{d}V + \int_s \rho\boldsymbol{\psi}\mathbf{U}\mathrm{d}\mathbf{S} = \int_\mathrm{V} \mathrm{Q}(\boldsymbol{\psi})\mathrm{dV} \qquad (25)$$

After approximating the source and convective terms of Eq. 25 its semi-discrete form is obtained:

$$\frac{\partial}{\partial t}\int_V \rho\boldsymbol{\psi}\mathrm{d}V + \sum_f \boldsymbol{\psi}_f F = Q(\boldsymbol{\psi})_p \mathrm{V}_p \qquad (26)$$

Here, F is the mass flux through the face ($F = \mathbf{S}\cdot(\rho\mathbf{U})_f$) and $\boldsymbol{\psi}_f$ is the transported variable reconstructed value. For source terms the simplest second order discretization can be obtained by approximating the volume integrals with the product of the integrand mean value by the cell volume.

In compressible fluids, properties may be transported by waves independently of the bulk flow. Therefore flux interpolations that take into account that transport processes can occur in any direction are required. Here convective terms are evaluated with the second order central-upwind scheme of Kurganov, Noelle and Petrova (KNP) [37].

Kurganov schemes are free Riemann solver techniques used for numerical flux approximation. These kind of schemes do not involve characteristics information on the construction of the numerical fluxes, and avoid exact Jacobian evaluations. Therefore this scheme is an interesting alternative to traditional methods based on Riemann solvers [4, 2, 5]. This family of schemes have been extensively tested in simulations of non-reactive high speeds flows achieving numerical solutions of comparable quality and considerably lower cost, than those obtained with traditional Riemann solvers [48, 25, 49]. The physical domain is discretized in finite volumes (cells) and internal faces are defined between proprietary (P) and neighbor (N) cells (Fig. 1). The face's vector $\mathbf{S}_f$ points outward from the inner surface. All dependent variables and thermophysical properties are stored in each cell's centroid (e.g. P in Fig. 1). The vector $\mathbf{d}_{PN}$ connects the centroid of cell P with that of neighboring cell N , and the vector $\mathbf{d}_{fN}$ connects the center of the inner face with the centroid of cell N. It is important to comment that regardless of the $1D$ context of the present work, the finite volumes discretization presented follows the OpenFOAM® philosophy. In consequence, it is done having in mind an arbitrary dimensional discretization in a complete unstructured framework. Taken care of inward and outward waves propagation at cell interfaces, numerical fluxes interpolation can be defined as [8]:

$$\phi_f\psi_f = \alpha_+\phi_{f+}\psi_{f+} + \alpha_-\phi_{f-}\psi_{f-} + \omega_f\left(\psi_{f-} - \psi_{f+}\right) \qquad (27)$$

which are then computed applying proper values (ψ_{f+},ψ_{f-}, α_+,α_- and ω)[3] provided for the KNP scheme [37, 25]. Given the good results obtained in [25] and [27] for non-reactive high-speed flow simulations, in the

[3] Subscripts + and − indicate outward and inward directions respectively.

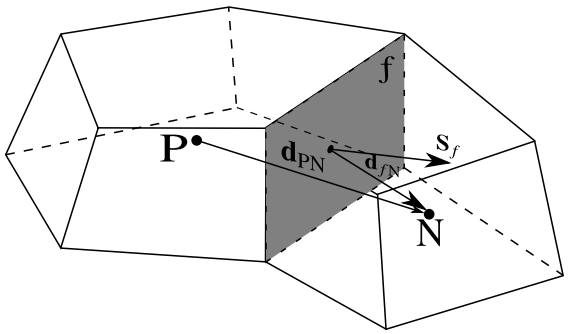

Figure 1: Finite volume discretization

computations performed here the van Leer limiter function is selected [50]. The only gradient involved term is ∇p (momentum equation), and it is evaluated with the KNP scheme [25], that guarantee a second order approximation. Temporal integration is performed in two steps, first all chemical concentrations are actualized, then source terms in energy and species equations are calculated and finally, the fluid-dynamic system is advanced in time. The chemical kinetic process is modeled with $N-1$ stiff ODEs. To obtain the $N-1$ species concentrations $[\mathbf{C}]$, the ODE system is evolved from $[\mathbf{C}]^{n-1}$ to $[\mathbf{C}]^{n}$ by using the semi-implicit mid-point rule of Bader and Deuflhard (SIBS) [40]. Numerical integration is starting by providing an initial chemical time step ($\Delta\tau^c$) and it is adaptively reduced to satisfy a tolerance 1×10^{-9}.

Once chemical system integration is done and source terms of energy and species equations are actualized, the complete set of discrete fluid-dynamic equations is evolved in time. Time evolution of the fluid-dynamic system is calculated with the forward Euler scheme. By integrating the left member of Eq. (26) the semi-discrete formulation is achieved [47]:

$$V\left((\rho\psi)^n-(\rho\psi)^{n-1}\right)=Q(\psi)_p\mathrm{V}_p-\sum_f\phi_f\psi_f \qquad (28)$$

Time advanced is controlled by the fluid dynamic integration time step Δt determined from the maximum Courant number $\max(C_o)$.

To develop the simulations, the computational domain has similarity with a shock tube, that is a long duct closed in both sides or open in one of them. The possible physical boundary conditions are: inlet, outlet or solid (impermeable) wall. For a supersonic inlet, all fields must be imposed. For an outlet, if the flow is supersonic all characteristics are outgoing, therefore, all fields must satisfy the von Neumann (zero gradient) condition

$$\left.\frac{\partial\mathbf{u}}{\partial\mathbf{n}}\right|_{\delta\Omega}=0 \qquad (29)$$

At a solid wall, and for any inviscid flow the velocity vector must be tangent to the surface, thus

$$\mathbf{U}\cdot\mathbf{n}=0 \qquad (30)$$

being $\mathbf{n}$ the unit normal vector to the wall. Note that others inlet and outlet flow conditions are not so straight to impose, therefore techniques based on characteristics must be used [51, 52].

4.3. Computational algorithm

In this section it is presented the computational algorithm. Before introducing the algorithm it is convenient to list the involved equations:

- Stiff ODE system related to chemical model
- Global mass conservation equation
- Momentum conservation equations
- Energy equation
- $N-1$ species conservation equations and its source terms

Algorithm 1 rhoCentralRfFoam

1: **procedure** (for $t_i < n_t$)
2: {
3: Read boundary and initial conditions for T, p, **U** and Y_i
4: Assemble and solve the ODE system related with the selected chemical model
5: Compute mixture thermo-physical properties
6: Compute source terms for species and energy equations
7: Compute necessary parameters to calculate numerical fluxes ($\alpha_{\pm}$, $\phi_{f_{\pm}}$, etc)
8: Assemble and solve rhoEqn.H (compute p*)
9: Assemble and solve UEqn.H
10: Assemble and solve Eeqn.H
11: **for** i=0;i<Y.size();i++
12: {
13: Assemble and solve YEqn.N
14: }
15: Calculate $Y_N = 1 - \sum Y_i$
16: Calculate p
17: }

- Thermal and caloric equations of state

The algorithm summary (Algorithm. 1) presented [53], has been written according to the C++ coding style recommended by OpenFOAM®. All equations are implemented in a header file and then, from the main source code `rhoCentralRfFoam`, each one is called.

Note that the ODE system associated with the chemical process is the first to be assembled and solved. Once the new species concentrations are known, its thermo-physical properties are actualized and source terms of species and energy transport equations are determined. Then the global continuity equation is solved and numerical fluxes are determined. Next an intermediate pressure field (p^*) is obtained and momentum and total energy equations are solved.

From the energy E (Eq. (5)), the sensible enthalpy h_s is obtained[4], then the temperature can be computed from h_s through a Newton-Raphson iterative technique.

At its last step the Algorithm 1 assembles and solve $N-1$ species equations and the pressure is actualized. The species N is determined by $Y_N = 1 - \sum^{N-1}(Y_i)$[5].

It is interesting to note that the solver `rhoCentralRfFoam` has been developed according to the OpenFOAM® philosophy, allowing the selection of the ODE solver, the fluid dynamic temporal integrator and limiter functions at run time. These features makes the solver very powerful in the sense that all available limiter functions can be used and the implementation of others time integrators does not involve substantial changes in the main code.

5. Chemical source terms and kinetics models

The chemistry is modeled utilizing three (3) kinetics models for $H_2 - O_2$ diluted mixtures combustion. Two models with 13 species 33 reactions belong to Jachimowski [30, 31] and the third one with 10 species and 25 reactions, to Marinov [32]. All models involve reactions of the form described by Eqs. (14)-(15). Reactions and its respective Arrhenius coefficients are listed in Appendix. A

[4] In high speed reactive flow simulations the total energy (E) is preferred because otherwise the formulations is not conservative, and therefore shock discontinuities are badly predicted [54, 55, 56]

[5] This species is taken as an inert one on the chemical model (i.e, He or Ar)

The species considered in Jachimowski (Table. A.1-Table. A.2) and Marinov (Table. A.3) kinetics models are:

J1988-1992:	N_2	H	H_2	H_2O	H_2O_2
	HNO	HO_2	N	NO	NO_2
	O	O_2	OH		

M1996:	H_2	H	O_2	O	OH
	HO_2	H_2O_2	H_2O	N_2	

In Appendix. A, third body efficiencies for each model are also listed.

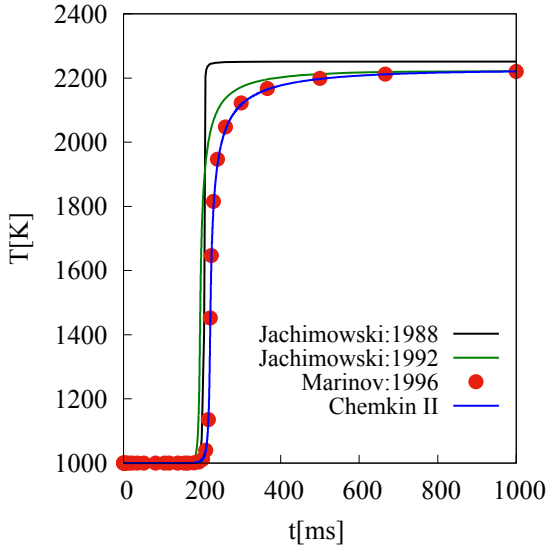

Figure 2: Temperature evolution in $H_2 - Air$ combustion ($\phi = 2.0$)

6. Chemical models validation

To select the most convenient chemical model for detonation simulations, the temperature time evolution from its initial value is compared with available data. The computation, performed under the assumption of a constant volume process, is done with a mixture $H_2 - Air$ ($\phi = 2$) and initial conditions $P_0 = 202650Pa$, $T_0 = 1000K$. To solve the stiff ODE system with SIBS, an initial chemical time step $\Delta\tau = 1.10^{-7}s$ is imposed and, it is updated to meet a specific tolerance (e.g. $\delta_r = 1.10^{-9}$). From typical temperature profiles as those displayed in Fig. 2, it has been concluded that numerical simulations performed using Marinov chemical kinetics, provide data that best compare with a reference profile taken from CHEMKIN [57]. Induction time (also known as ignition delay), can be defined as the necessary time to build a radical population capable of promoting the combustible mixture ignition. During the induction time important chemical reactions take place while the temperature remains nearly constant. However, the precise definition of induction time depends on the criterion used, consequently there are many formulated an accepted criteria [58]: formation of intermediate products OH or CO, values of increased pressure or temperature, etc. Two criteria have been formulated in this work: 5% increased temperature above the mixture initial value and maximum value of OH. In addition, the time to reach 95% of the reaction maximum temperature has also been computed. The time associated with this 95%, has to be interpreted as a boundary that must not be exceeded on any criteria.

A computation is performed in a $H_2 - O_2$ stoichiometric mixture diluted with Ar ($2H_2 : O_2 : 7Ar$), pressure 131700 Pa and temperature in the range 1000 K – 2000 K. Fig. 3 shows induction times obtained which each criterion described here and referenced numerical data provided by [59, 60]. The 5% criteria seems to be the best suited and the max(OH) the least appropriate.

To confirm the above statement a new test case with available experimental data, is run. The experimental induction times were measured in a shock tube using the reflected shock technique, the mixture was $2H_2 : O_2$

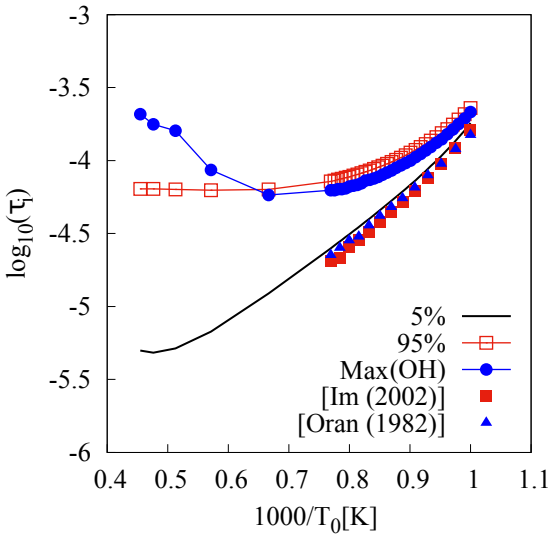

Figure 3: Induction time in combustible mixture $2H_2 : O_2 : 7Ar$ ($\phi = 1.0$; $p_u = 1.3\,atm$)

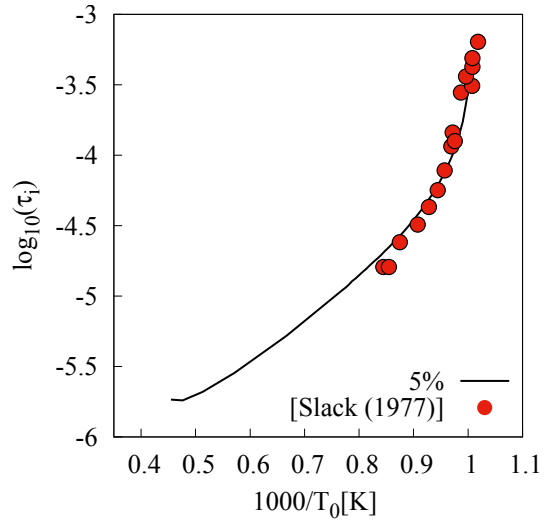

Figure 4: Induction time in combustible mixture $2H_2 : O_2$ ($\phi = 1.0$; $p_u = 2\,atm$)

and the pressure p = 202650 Pa (2 atm). In Fig. 4, it can be seen that computed induction times with the 5% criterion are in good agreement with the experimental data from [62]. It shall be remember, that a good prediction of the induction time is important because it has a strong influence on the mesh resolution needed to properly capture dynamic detonations parameters, and cellular structures [1]. In Fig 5, a set of numerical and experimental data on induction times related to $H_2 - O_2 - N_2$ and $H_2 - O_2 - Ar$ mixtures compiled by Elhsnawi et al. [61], is presented. Induction times satisfying the 5% criterion ($p = 0.1MPa$), computed in this work are also included.

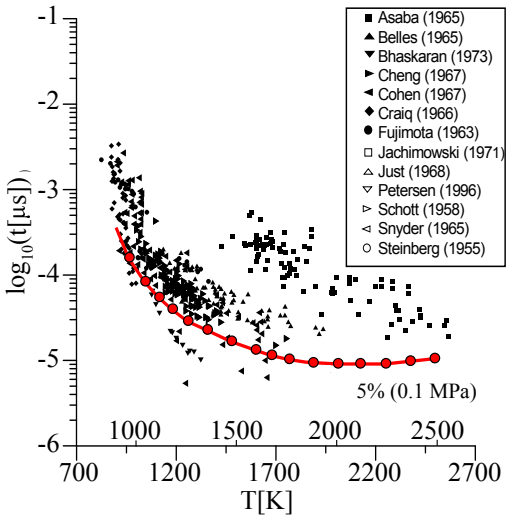

Figure 5: Induction time results compared with 5% criterion applied to $H_2 - O_2$ ($\phi = 1; 0.1MPa$) combustible mixture (Available data for different mixtures and conditions taken from [61] for $[H_2 : O_2 : Ar : N_2, (700K \leq T \leq 2700), (0.015MPa \leq p \leq 8.7MPa), (0.06 \leq \phi \leq 9)]$)

It can be seen that with initial temperatures at least up to $1300K$, an acceptable agreement between the available data of Fig 5 and the 5% criterion results, exists. As the temperature initial value increases, the dispersion of compiled data is such (one order of magnitude or more), that perhaps the 5% criterion may seem very optimistic. However, it can be interpreted as an indicator that ignition of the fuel-oxidizer given mixture, may take place.

7. Detonations test cases

This section presents four test cases of detonation processes, each one showing different features. The objective of these simulations is to analyze the capacity of `rhoCentralRfFoam` to predict detonation parameters and properties in the context of one-dimensional approximation.

7.1. Hydrogen-air planar detonation

The first test case to be considered, is the planar detonation induced in a stoichiometric mixture of $H_2 - Air$. The initial configuration can be seen in Fig. 6, in which a driver filled with high pressure and temperature helium is used to start the detonation. Igniter (driver), fresh mixture (driven) and burned gases are identified by the subscripts D, u and b respectively. The computational domain has a total length (L) of $0.5m$, the driver length is $L_D = 50\,mm$ and the entire domain is discretized using 1000 cells ($\Delta x = 0.5mm$). The driver and driven initial conditions are listed in Table. 1.

All results obtained with `rhoCentralRfFoam` employing different chemical models, will be compared one with another to study the impact of chemical kinetics modeling. In addition, to verify the behavior of `rhoCentralRfFoam`, results for pressure, temperature, density, and water formation are compared with profiles computed with the `FlowTwo` code[2]. `FlowTwo` is a genuine one-dimensional code that uses an implicit technique [63] and a second order Harten-Yee TVD scheme in a finite volume discretized domain [64]. All calculations are developed in parallel with 4 processors, resulting in a computation time of 3 hours per case. At the left of the domain solid wall boundary conditions are imposed (zero gradient for T and p, and zero velocity), and

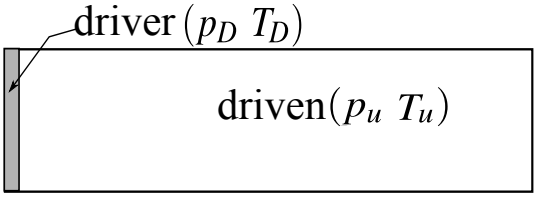

Figure 6: Shock tube initial configuration

Var.	Driver	Driven
p	2MPa	0.02Mpa
T	3000.0	300
U	$(0,0,0)$	$(0,0,0)$
$Y(N_2)$	0.0	0.7452
$Y(H_2)$	0.0	0.0283
$Y(H_e)$	1.0	0.0
$Y(O_2)$	0.0	0.2265

Table 1: Initial conditions: H_2 - Air ($\phi = 1.0$) detonative mixture. High pressure and temperature helium igniter

the right boundary being considered an outlet, all variable are extrapolated from internal fields. After applying the splitting technique, a maximum Courant number of 0.25 ($\Delta t = 3.08 \times 10^{-1} s$) is imposed in solving Euler equations using `rhoCentralRfFoam`. Typical results (pressure, temperature, density and water mass fraction) obtained after $t = 228\mu s$ are plotted in Fig. 7. The results obtained with Jachimowski (1988-1992) and Marinov (1996) chemical models are compared one with each other. It may be noticed that results produced by `rhoCentralRfFoam` using the Jachimowski's (1988) chemical model differ substantially from the other two. However, it is observed that the computations developed with `rhoCentralRfFoam`, and `flowTwo` with both using the Jachimowski's 1992 model are in good agreement. In Fig 8 are plotted the behavior of certain species also at $t = 228\mu s$ after the process started. The abrupt

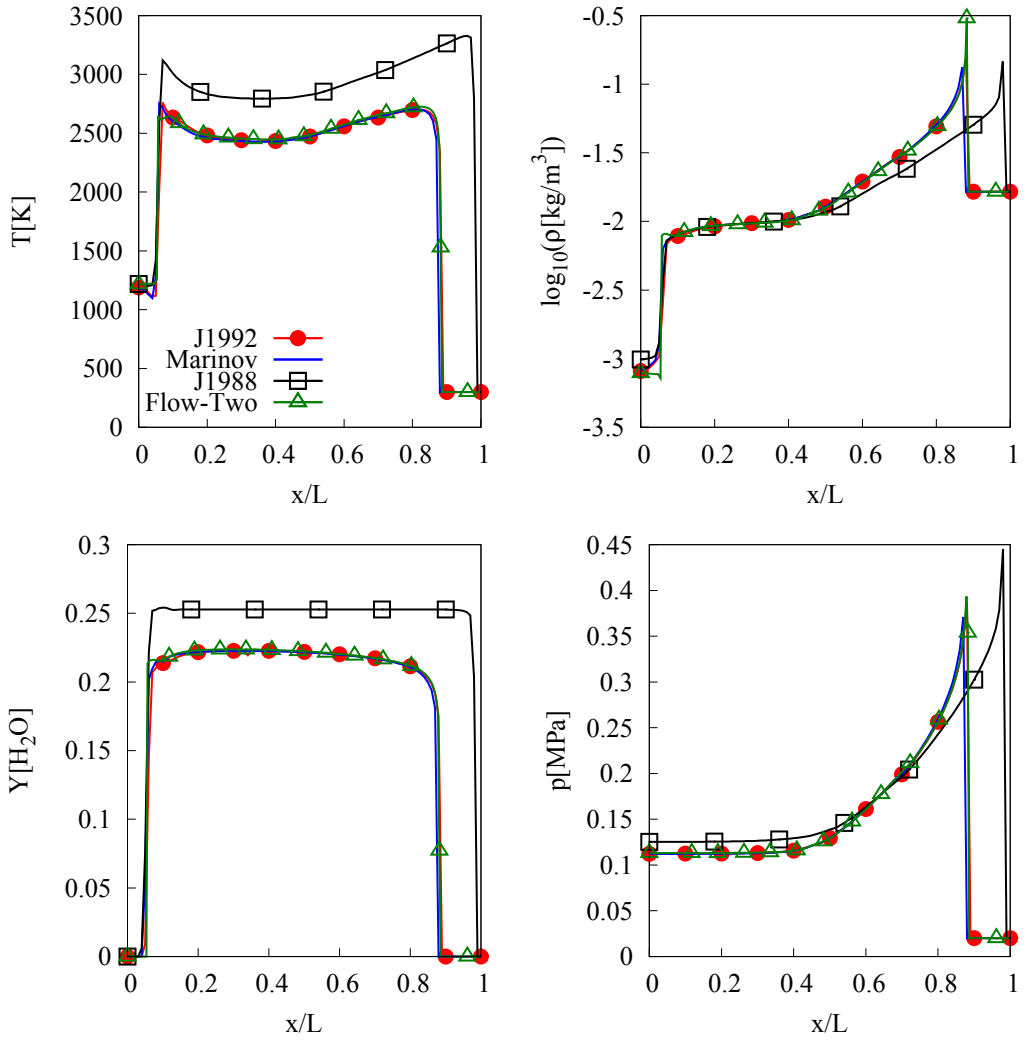

Figure 7: Pressure, temperature, density and water distributions for each kinetics model at $t = 228.4\mu s$. $H_2 - Air$ ($\phi = 1$) detonative mixture

change in species concentrations at the detonation front and at the contact surface between He and the reaction products, they by themselves, say about the potential of the solver `rhoCentralRfFoam` in treating discontinuities. Detonation propagation velocities (D) should be approaching to the Chapman-Jouguet (CJ) value ($D^{CJ} = 1933.8^{m}/_{s}$), for $H_2 - Air$ stoichiometric mixture [65]. In Table.2 values of propagating velocity for each kinetic model are presented, it can be observed that Jachimowski 1992 and Marinov models give the best predictions for detonation speed D.

Chemical model	$D[^{m}/_{s}]$	%Error
Jachimowski-1988	2145.6	10.4
Jachimowski-1992	1926.7	0.37
Marinov-1996	1904.8	0.5

Table 2: Percentage error of simulated detonation velocity D, compared to CJ speed (H_2-Air, $\phi = 1.0$)

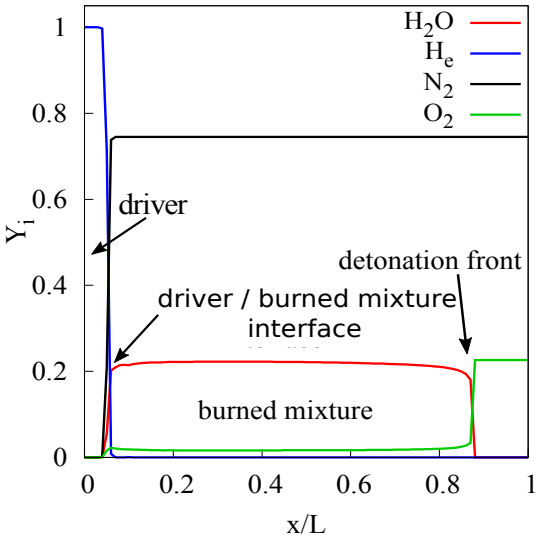

Figure 8: Species distribution obtained using Marinov model (t = 228.4μs). H_2-Air (ϕ = 1.0) detonative mixture

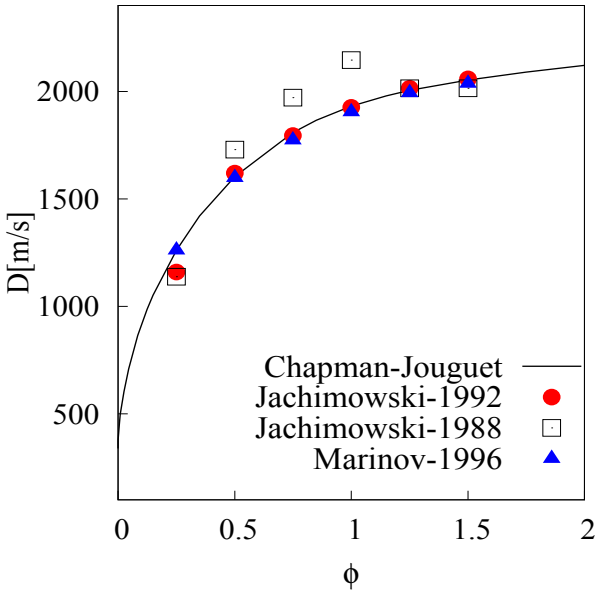

Figure 9: Detonation propagation velocity as function of equivalence ratios H_2 − Air detonative mixture

7.2. *Detonation velocity as function of equivalence ratio*

Again the H_2 − Air mixture is utilized, but now the equivalence ratio (ϕ) varies from 0.25 to 1.5 ($\Delta\phi$ = 0.25). Mixture compositions for each case are given in Table. 3. After performing simulations of six equivalence ratios for each chemical model, the resulting detonation velocities are plotted in Fig. 9, and are compared with CJ equilibrium calculations with the code CEA [65]. From Fig. 9 it is clear that Jachimowski 1992 and Marinov models predicts values in good agreement with the Chapman-Jouguet equilibrium values. Once more, the values predicted with the Jachimowski's 1988 model do not correlate properly with such values and, it can be observed that as ϕ increases the differences become larger. This proves as expected, that an appropriate kinetic model selection is decisive for a correct detonation speed calculation. Considering that Jachimowski's 1992 model and Marinov model give the best results, but Marinov model works with less reactions and species, in all simulations to come the Marinov model is going to be used.

ϕ	Y_{H_2}	Y_{O_2}	Y_{N_2}
0.25	0.00728	0.231	0.761
0.5	0.01446	0.229	0.756
0.75	0.02153	0.227	0.750
1.0	0.02851	0.226	0.745
1.25	0.03538	0.224	0.739
1.5	0.04216	0.223	0.734

Table 3: Mass fraction composition for H_2-Air mixture as function of equivalence ratio (ϕ)

7.3. *On the one-dimensional structure of a detonation*

The Chapman-Jouguet (CJ) theory does not provide any information about the structure of the detonation processes, it only gives information about static parameters (p_b/p_u, T_b/T_u, ρ_b/ρ_u, D and equilibrium

composition)[6] [1]. However, the ZND (Zeldovich, von Neumann and Döring) theory, admits time dependent chemical reactions and so, several sequential stages carried on with the detonation process, can be shown. First, an infinitely thin shock wave compresses the combustible mixture to a high pressure known as the *von Neumann spike*. This spike marks the onset of the strongest exothermic chemical reactions region, which should be completed at the CJ state point. From this point, detonation products begin to expand backwards [66, 67, 68].

To verify the existence of a ZND one-dimensional structure in detonations computed using `rhoCentralRfFoam` code, a stoichiometric mixture of $H_2 - O_2$ with 70% Argon dilution ($2H_2 : O_2 : 7Ar$), is considered. The unreacted conditions of this mixture are: $2H_2 : O_2 : 7Ar$, $p_u = 6670.0$Pa and $T_u = 298.0K$. The driver conditions are: $p_D = 1.5$ MPa and $T_D = 3800\,K$.

When the CJ propagation velocity is exceeded, a detonation is known as strong or overdriven. In this case, relations applicable to strong non stationary shocks can be utilized to obtain flow conditions at the von Neumann spike [67]. The `rhoCentralRfFoam` computed detonation velocity is $\sim 1640\,m/s$, close enough to the value of $\sim 1616.3\,m/s$ provided by the CEA equilibrium calculation. The computed pressure and temperature at von Neumann spike are: $p_{vN} = 173613.6$ Pa and $T_{vN} = 1967K$[7]. Now, by applying the 5% criteria; the calculated induction time is $\tau_i = 3.73\mu s$. In a fixed frame of reference, the gas velocity behind the spike is $u_{vN} = 1264.5^m/_s$, therefore the gas velocity relative to the front is evaluated as

$$V_{vN} = D - u_{vN} = 351.83^m/_s \tag{31}$$

with this value of V_{vN}, the induction length is computed ($L_i = V_{vN}\tau_i$, $L_i \approx 1.312mm$). This result is in fair agreement with values reported in other studies for the same mixture and conditions (i.e, Oran et al. $L_i = 2mm$, [69] and Deiterding $L_i = 1.4mm$ [5]). To ensure a proper resolution a grid with $13pts/L_i$ is used, therefore a mesh with $N_c \sim 10000$ pts. per meter is needed. At the left a solid wall limit is imposed and at the right, if needed, an outlet type boundary has to be considered. In Fig. 10

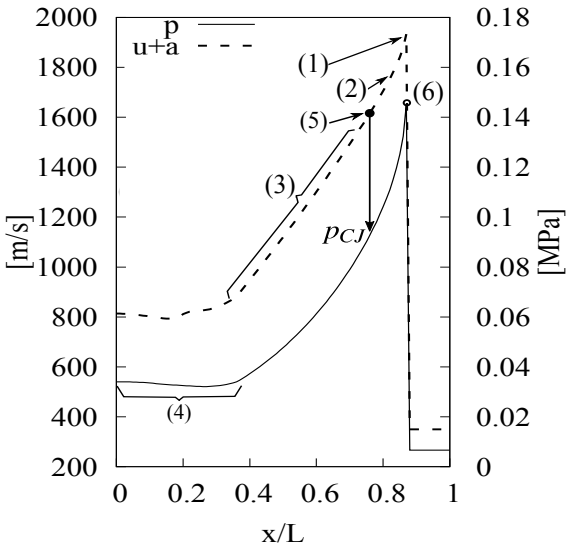

Figure 10: $u + a$ and p profiles $2H_2 : O_2 : 7Ar$ detonative mixture ((1) Induction zone; (2) Strong reaction zone; (3) Reaction zone; (4) Steady state zone; (5) Chapman-Jouguet point; (6) von Neumann spike)

show typical ZND profiles, in which $u + a$ (sum of flow speed with corresponding speed of sound), and pressure are plotted versus distance. There is a particular value of $u + a$, where such amount equals the speed of CJ detonation. In Fig. 10 four zones are identified: Induction zone ($L_i = 1.31\,mm$) (1), the end of this zone marks the

[6] Subscript b means burned mixture and u unburned. D is detonation velocity

[7] The subscript vN indicated any property related to von Neumann spike

onset of strong exothermic chemical reactions; Strong reaction zone (2), where the exothermic reactions are taking place; Reaction zone (3), where theoretically the chemical equilibrium is reached with less intense reactions than in zone (2); Steady zone (4) where the reactive process has finished and the flow properties have reached, supposedly, the equilibrium state.

Values for pressure at von Neumann spike and CJ point can be obtained from Fig. 10: $p_{CJ} = 92722\,\text{Pa}$ and $p_{vN} = 1.6p_{CJ}$. The pressure computed value at CJ point is in good agreement with the experimental data of 94000 Pa [3]. At the von Neumann spike the value that the theory predict is $p_{vN} = 1.8p_{CJ}$. It is believed that the agreement in p_{vN} can be improved if a higher mesh resolution is used near by the von Neumann spike. In Table. 4 the values obtained at zone (4) are compared with the equilibrium results computed by CEA code [65]. In

Y_i	CEA	rhoCentralRfFoam
O_2	0.0108	0.0154
H_2	0.00193	0.0023
H_2O	0.0871	0.0801
OH	0.01118	0.01059
Ar	0.88589	0.88589

Table 4: Equilibrium compositions at zone 4 ($2H_2 : O_2 : 7Ar$ detonative mixture)

Fig. 11 detonation front positions vs.time are plotted. In the case that is shown in Fig. 11(a,b), driver and driven are filled with the same reacting mixture, while in Fig. 11(c,d) the driver is filled with Helium. In the case in which driver and driven are filled with the same reacting mixture a weak discontinuity (Fig. 11b) behind the front can be detected. When the driver gas is changed to Helium, the interface between driven and reacting zone is more clearly distinguished (Fig 11d), and expands less not exceeding 3 times the initial driver length.

7.3.1. On the convergence of overdriven detonations toward the CJ state

If the initiation energy is very strong, the initial detonation speed (D) is greater than the corresponding Chapman-Jouguet (D_{CJ}) detonation speed ($D > D_{CJ}$), then it is said that detonation is overdriven. Unless especial starting configurations are imposed [2], an overdriven detonation will always show tendency to becomes a Chapman-Jouguet detonation. The distance needed for an overdriven wave to approach the CJ detonation value, varies depending on physical properties that distinguish the gas in the driver (or initiator) from the fuel in the driven without burning. Mainly, due to differences in the speed of sound. Furthermore, if such difference is very large as it may results using high temperature He as driver gas, the detonation speed could even go underdriven if compared with equilibrium CJ value. Typical results obtained showing the behavior of propagating detonations waves are shown in Fig. 12. Plot a in Fig. 12, has been built using a $2H_2 : O_2 : 7Ar$ driver mixture, burned and overheated to reach a sound speed of $1098.5 m/s$, that is ~ 2.11 times greater than the speed of sound of the driven fuel mixture without burning, which also is $2H_2 : O_2 : 7Ar$. It clearly shows how an overdriven detonation approximates the CJ speed of $\sim 1616\, m/s$ (computed using CEA [65]).

Consider now Plot b in Fig. 12, obtained with a heated He driver whose sound speed is $3627\, m/s$, that is ~ 6.97 times greater than the sound speed of driven fuel without undergoing combustion. It can be seen the detonation front going quickly underdriven by a small amount, but noticeable. However, it is not clear if it will remain

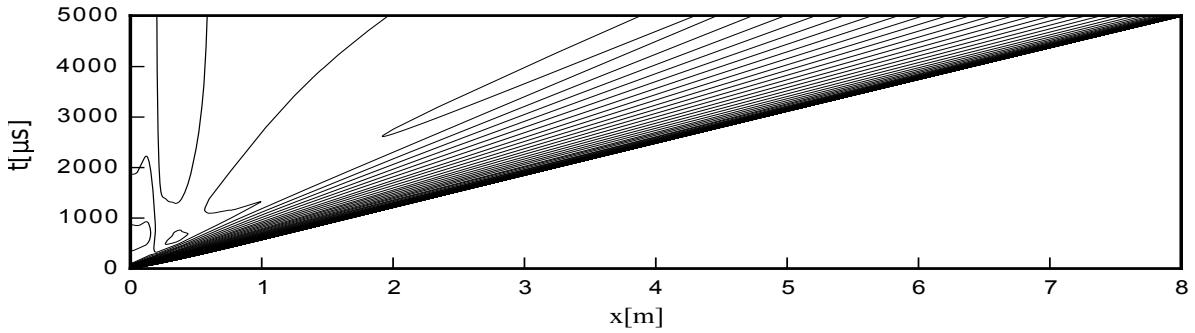

(a) $[0, 8]m \times [0, 5000]\mu s$ (Driver: $2H_2 : O_2 : 7Ar$)

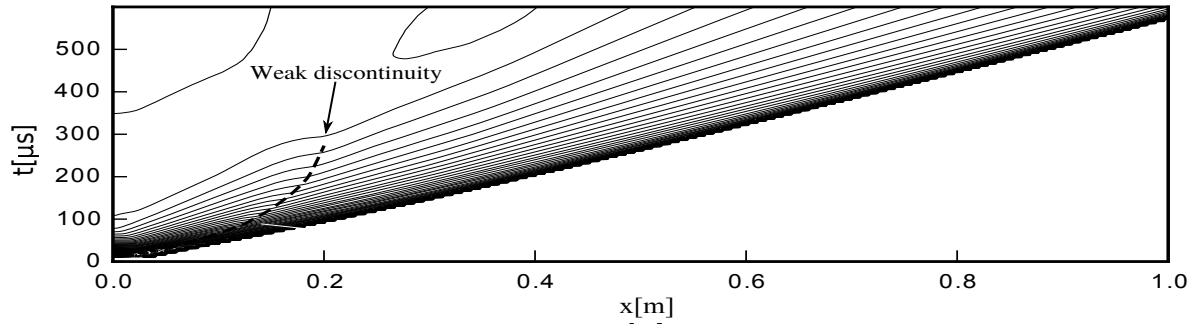

(b) $[0, 1]m \times [0, 600]\mu s$ (Driver: $2H_2 : O_2 : 7Ar$)

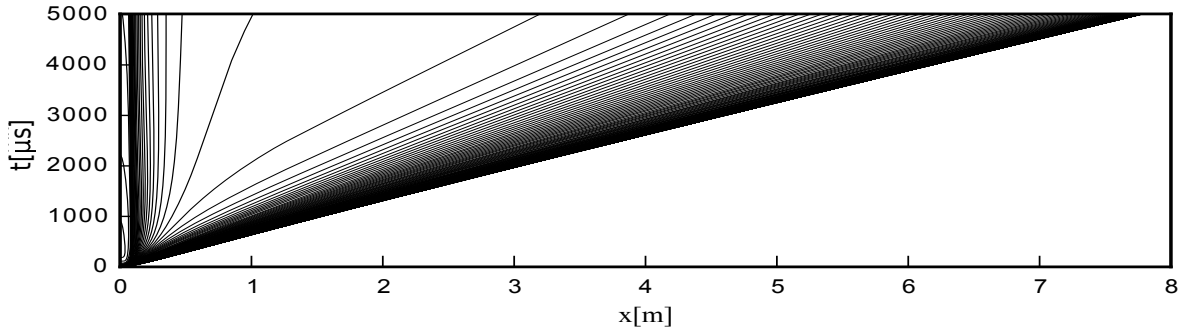

(c) $[0, 8]m \times [0, 5000]\mu s$ (Driver: He)

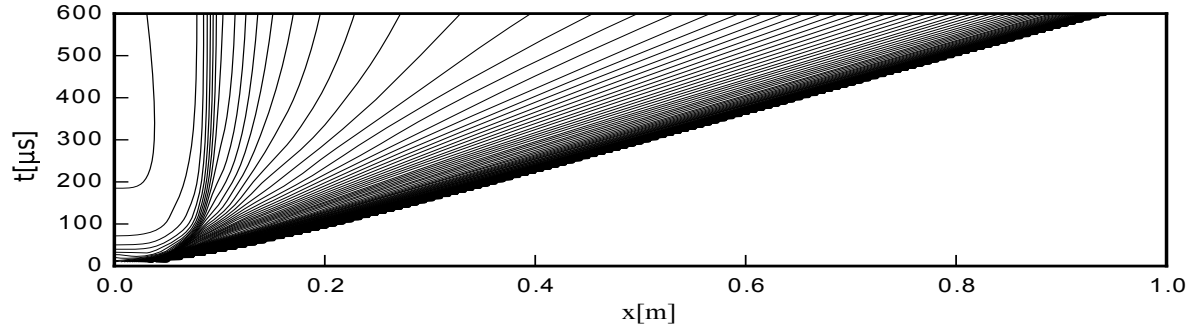

(d) $[0, 1]m \times [0, 600]\mu s$ (Driver: He)

Figure 11: t vs. x detonation contour plots for $2H_2 : O_2 : 7Ar$ reacting mixture (Drivers: $2H_2 : O_2 : 7Ar$ and H_e)

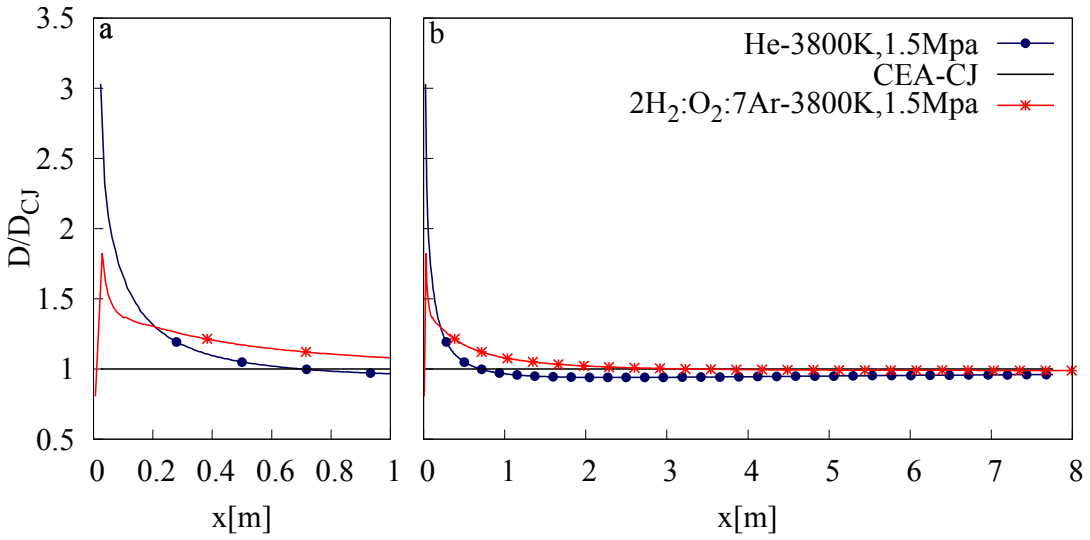

Figure 12: Convergence toward the Chapman-Jouguet propagation velocity

underdriven forever, or it is approaching very slowly to previously accepted CJ value ($\sim 1616\,m/s$), or simply, it converges to a new CJ speed of $\sim 1553\,m/s$ (3.8% lower value). For the moment, there is not an answer for this apparent ambiguity.

7.4. Ignition by a shock wave reflexion

The induction time (τ_i) can be measured by reflected shock experiments. The experimental technique used comprise simultaneous measurements of pressure, UV light transmission (either only emission or emission plus absorption), and recording through time-resolved schlieren pictures of the shock reflection and the reaction wave formation. The shock tube facility and technique for taking time-resolved schlieren pictures have been described in detail by Strehlow and Cohen [70]. Here the ignition test case for a mixture of $2H_2 : O_2 : 7Ar$ studied in [59] and [60], is simulated. In Table. 5 there are given flow conditions behind the incident shock wave and computed field conditions between wall and reflected shock. Fig. 13 shows the geometry

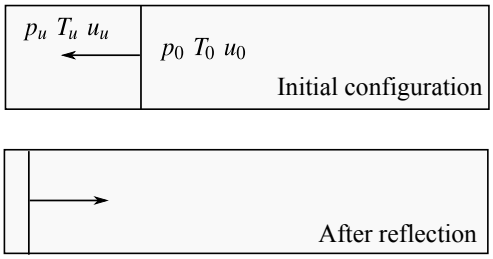

Figure 13: Ignition by a reflected shock wave. Test case configurations

Field	Incident shock	Reflected shock (computed values)
p [Pa]	36679.65	130634
T[K]	624	1035.3
u[m/s]	-478.5	0

Table 5: Ignition by a shock wave reflexion initial conditions

and general configuration used to simulate the experiment. The calculation is done in a domain $0.5m$ long and it is initialized with an incident shock moving from right to left. A mesh with 6000 cells is employed, the Courant number is limited to 0.1 and the van Leer limiter function is utilized in all reconstruction procedures. At the left wall, boundary conditions imposed are zero gradient for T and p, and zero velocity. The right boundary behaves like an inlet with flow conditions to ensure the intensity of the incident shock satisfying the jump conditions $\mathrm{p}_u, T_u, 0 \rightarrow \mathrm{p}_0, T_0, u_0$ ($\mathrm{p}_\mathrm{u} = 6670Pa$ and $T_u = 298K$ (Table. 5). In Fig.14, constant contour lines of temperature obtained from numerical simulation are presented in a time vs. distance plot. All involved waves have been clearly detected: the reflected shock from the wall (1), the starting and build up of the reaction wave (2), the transmitted detonation (4), a contact discontinuity (5) and a matching wave (3) starting where the reaction wave merges with the reflected shock, travels toward the wall and becomes reflected. Also, a schlieren picture taken from experiments reported in [59], is attached on the right side. It can be seen that all waves above listed, can be identified in the experimental figure. There is disagreement regarding the formation of the reaction wave (2) and on the time it interacts with reflected shock (1). It is suspected that they are consequences of differences between the kinetic model employed in this paper and the one used in the reference. Nevertheless, two criteria used to define induction times τ_i are here evaluated: Oran et. al. [59] based on $20K$ degree increase above the initial temperature, and the one here proposed based on 5% temperature increase. The corresponding values are: $\sim 116\mu s$ (Oran prediction is $110\mu s$), and $\sim 123\mu s$ respectively. Fig. 15 shows how the value of $\tau_i = 123\mu s$, is in satisfactory agreement with the experimental data obtained by Oran et al. The 95% temperature increase shows when the reaction wave starts to develop and changes its speed with traveled distance, however it does not reach the CJ equilibrium value $1616.3ms^{-1}$(CEA) [65].

In Fig. 16 pressure, temperature and water formation profiles at $t = 163\mu s$ and $t = 307.5\mu s$ are shown. At $t = 163\mu s$ profiles corresponding to an early time formation of the reaction wave are plotted. At $t = 307.5\mu s$ the reaction wave has already overcomes the reflected wave and the transmitted detonation structure can be observed. Such transmitted detonation is clearly more intense (higher pressure peak), than the starting reaction wave (2).

8. Conclusions and future work

In this paper, a new solver, evolution of `rhoCentralFoam` and renamed `rhoCentralRfFoam`, is presented. It was built using the finite volume framework of OpenFOAM®, the KNP central scheme to deal with convective fluxes and detailed chemical kinetics to describe the occurrence, structure and propagation of planar detonations in combustible mixtures. The SIBS technique to solve the stiff ODEs system needed to compute sources for production/consumption of reacting species and the progression of the overall heat released, is also added. Based on the results obtained, it can be concluded that KNP scheme provide a good and reliable alternative of traditional methods based on Riemann solvers and besides, does the job in shorter computational times. Comparison with results computed with the code `Flow-Two` which uses a Harten-Yee (TVD) scheme, have shown good agreement and discrepancies were due mainly, to differences

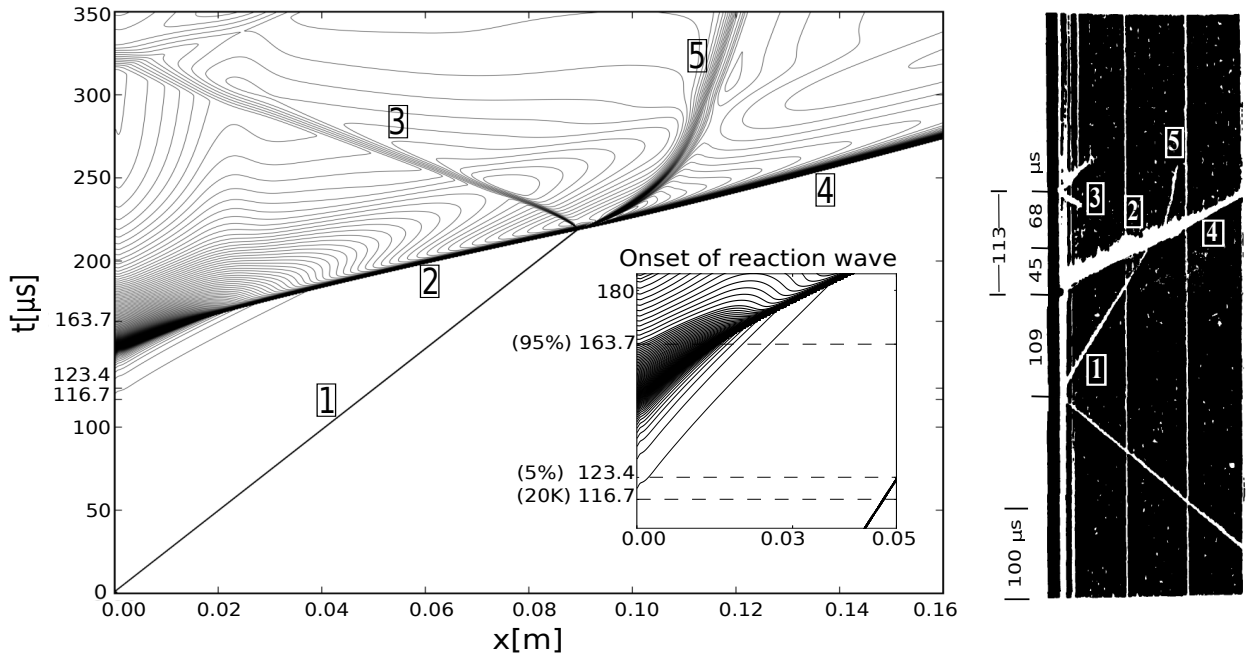

Figure 14: Comparison of wave interactions with experimental data (taken from [59]) (1. Reflected shock; 2. Reaction wave; 3. Matching wave; 4. Transmitted detonation; 5. Contact discontinuity)

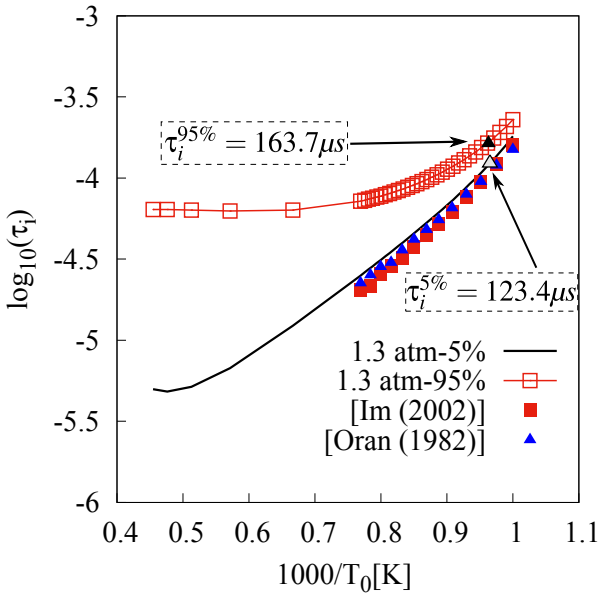

Figure 15: Constant volume induction time computation

on the chemical kinetics. The correct selection of the kinetics play a key role on the prediction of detonation propagation velocity and hence, on describing its properties. Aspects of the ZND planar detonation model, such as the von Neumann pressure peak, the flow conditions at the CJ point, and all sequential stages before reaching the equilibrium condition, have been computed and good correlations with theoretical ZND values are obtained. However, discrepancies are found with final equilibrium compositions, most likely, in the simulations with `rhoCentralRfFoam` the equilibrium state has not been reached yet. The convergence from overdriven condition towards the Chapman-Jouguet state is proved. The `rhoCentralRfFoam` solver capacity to describe the onset of chemical reactions (induction time) behind the reflected shock, and interactions between all existent waves, it has also be

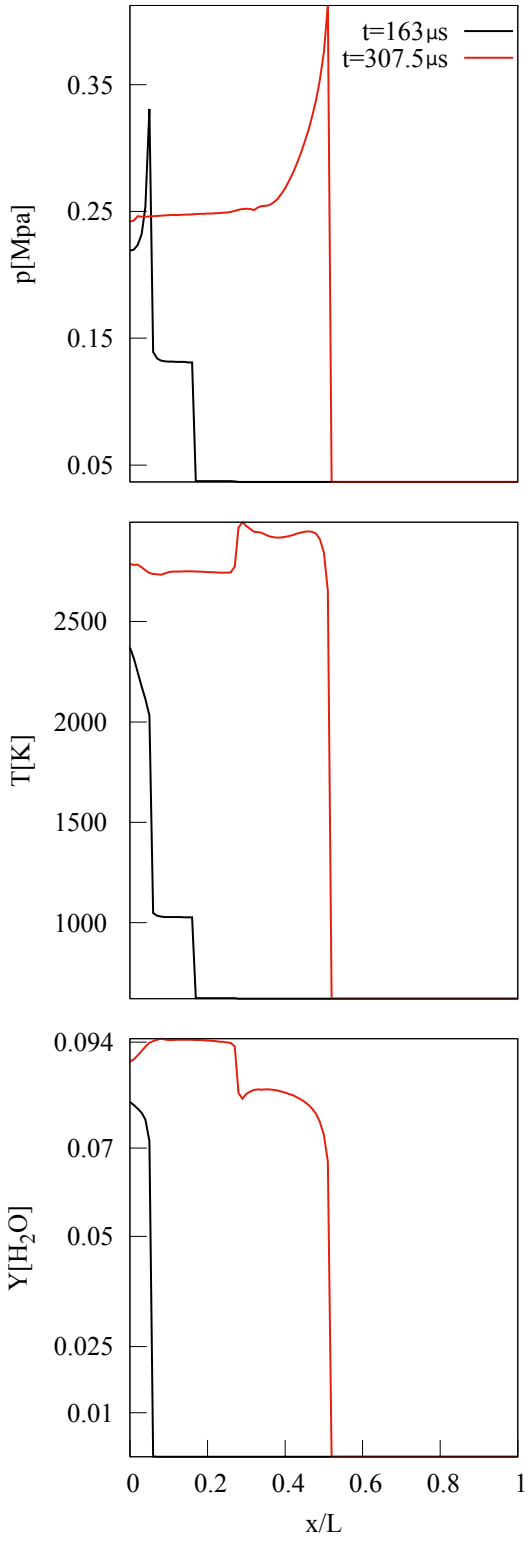

Figure 16: Pressure, temperature and water profiles at $t = 163\mu s$ and $t = 307.5\mu s$

proved.

As a continuation of this work, it is intended to compute 2D simulations to show that `rhoCentralRfFoam` can capture cellular structures in detonations. To improve 2D simulations quality without increasing the number of cells to unpractical situations, the moving-adaptive mesh capability will be incorporated and it will be done based on the work of Espinoza et al. [71], available in OpenFOAM® libraries.

It is also intended to use other types of fuels, mainly based on hydrocarbons. To improve temporal accuracy, higher order integrators are going to be implemented (e.g. TVD Runge-Kutta technique [72]). In addition attempts will be made to include in 2D simulations the turbulence using averaged type standard models.

Acknowledgements

This work was supported by CONICET, SECyT-UNC and MCyT Córdoba.

A. Chemical kinetics models

The Arrhenius coefficients and third body efficiencies for each chemical model are listed in Table.A.1,Table. A.2, Table. A.3 and Table. A.4.

Reaction	A	b	Ea
(1) H2 + O2 ⇆ OH + OH	1.7e13	0.0	48000
(2) H + O2 ⇆ OH + O	2.6E+14	0.0	16800
(3) O + H2 ⇆ OH + H	1.8E+10	1.0	8900
(4) OH + H2 ⇆ H2O + H	2.2E+13	0.0	5150
(5) OH + OH ⇆ H2O + O	6.3E+12	0.0	1090
(6) H + OH + M ⇆ H2O + M	2.2E+22	-2.0	0.0000
(7) H + H + M ⇆ H2 + M	6.4E+17	-1.0	0.0000
(8) H + O + M ⇆ OH + M	6.0E+16	-0.6	0.0000
(9) H + O2 + M ⇆ HO2 + M	2.10E+15	0.0	-1000
(10) HO2 + H ⇆ H2 + O2	1.30E+13	0.0	0.0000
(11) HO2 + H ⇆ OH + OH	1.40E+14	0.0	1080
(12) HO2 + H ⇆ H2O + O	1.00E+13	0.0	1080
(13) HO2 + O ⇆ O2 + OH	1.5E+13	0.0	950
(14) HO2 + OH ⇆ H2O + O2	8.0E+12	0.0	0.0000
(15) HO2 + HO2 ⇆ H2O2 + O2	2.0E+12	0.0	0.0000
(16) H + H2O2 ⇆ H2 + HO2	1.4E+12	0.0	3600
(17) O + H2O2 ⇆ OH + HO2	1.4E+13	0.0	6400.0
(18) OH + H2O2 ⇆ H2O + HO2	6.1+E12	0.0	1430.0
(19) H2O2 + M ⇆ OH + OH + M	1.2E+17	0.0	45500
(20) O + O + M ⇆ O2 + M	6.0e+17	0.0	-1800.00
(21) N + N + M ⇆ N2 + M	2.8E+17	-0.75	0.0
(22) N + O2 ⇆ NO + O	6.4E+9	1.0	6300.0
(23) N + NO ⇆ N2 + O	1.6E+13	0.0	0.0000
(24) N + OH ⇆ NO + H	6.3E+11	0.5	0.0
(25) H + NO + M ⇆ HNO + M	5.4E+15	0.0	-600
(26) H + HNO ⇆ NO + H2	4.8E+12	0.0	0.0000
(27) O + HNO ⇆ NO + OH	5.0E+11	0.5	0.0000
(28) OH + HNO ⇆ NO + H2O	3.6E+13	0.0	0.0000
(29) HO2 + HNO ⇆ NO + H2O2	2.0E+12	0.0	0.0
(30) HO2 + NO ⇆ NO2 + OH	3.4E+12	0.0	-260
(31) H + NO2 ⇆ NO + OH	3.5E+14	0.0	1500.0
(32) O + NO2 ⇆ NO + O2	1.0E+13	0.0	600.0
(33) NO2 + M ⇆ NO + O + M	1.16E+16	0.0	66000

Table A.1: Jachimowski 1988 chemical kinetic model [units: s, mol, cm^3, cal and K]

Reaction	A	b	Ea
(1) H2 + O2 ⇆ HO2 + H	7.0e13	0.0	56800.0
(2) H + O2 ⇆ OH + O	2.20E+14	0.0	16800.0
(3) O + H2 ⇆ OH + H	5.06E+4	2.67	6290.0
(4) OH + H2 ⇆ H2O + H	2.16e+8	1.51	3430.0
(5) OH + OH ⇆ H2O + O	1.50E+9	1.14	0.0000
(6) H + OH + M ⇆ H2O + M	8.62E+21	-2.0	0.0000
(7) H + H + M ⇆ H2 + M	7.3E+17	-1.0	0.0000
(8) H + O + M ⇆ OH + M	2.6E+16	-0.6	0.0000
(9) O + O + M ⇆ O2 + M	1.10E+17	-1.0	0.0000
(10) H + O2 + M ⇆ HO2 + M	2.30E+18	-1.0	0.0000
(11) HO2 + H ⇆ OH + OH	1.50E+14	0.0	1000.0
(12) HO2 + O ⇆ O2 + OH	2.00E+13	0.0	0.0000
(13) HO2 + OH ⇆ H2O + O2	2.0E+13	0.0	0.0000
(14) HO2 + HO2 ⇆ H2O2 + O2	2.0E+12	0.0	0.0000
(15) H + H2O2 ⇆ H2 + HO2	1.7E+12	0.0	3780.0
(16) H + H2O2 ⇆ OH + H2O	1.0E+13	0.0	3580.0
(17) O + H2O2 ⇆ OH + HO2	2.8E+13	0.0	6400.0
(18) OH + H2O2 ⇆ H2O + HO2	7.0E+12	0.0	1435.0
(19) OH + OH + M ⇆ H2O2 + M	1.6E+22	-2.0	0.0000
(20) N + N + M ⇆ N2 + M	2.8e+17	-0.8	0.0000
(21) N + O2 ⇆ NO + O	6.4E+9	1.0	6300.0
(22) N + NO ⇆ N2 + O	1.6E+13	0.0	0.0000
(23) N + OH ⇆ NO + H	6.3E+11	0.5	0.0000
(24) H + NO + M ⇆ HNO + M	5.4E+15	0.0	-600.0
(25) H + HNO ⇆ NO + H2	4.8E+12	0.0	0.0000
(26) O + HNO ⇆ NO + OH	5.0E+11	0.5	0.0000
(27) OH + HNO ⇆ NO + H2O	3.6E+13	0.0	0.0000
(28) HO2 + HNO ⇆ NO + H2O2	2.0E+12	0.0	0.0000
(29) HO2 + NO ⇆ NO2 + OH	3.4E+12	0.0	-260.0
(30) HO2 + NO ⇆ HNO + O2	2.0E+11	0.0	1000.0
(31) H + NO2 ⇆ NO + OH	3.5E+14	0.0	1500.0
(32) O + NO2 ⇆ NO + O2	1.0E+13	0.0	600.0
(33) NO2 + M ⇆ NO + O + M	1.16E+16	0.0	66000

Table A.2: Jachimowski 1992 chemical kinetic model [units: s, mol, cm^3, cal and K]

Reaction	A	b	Ea
(1) OH + H2 ⇆ H + H2O	2.14E+08	1.52	3449.0
(2) O + OH ⇆ O2 + H	2.02E+14	-0.4	0.0
(3) O + H2 ⇆ OH + H	5.06E+04	2.67	6290.0
(4) H + O2(+M) ⇆ HO2(+M)	4.52E+13	0.0	0.0
Low	1.05E+19	-1.257	0.0
(5) H + O2(+N2) ⇆ HO2(+N2)	4.52E+13	0.0	0.0
Low	2.03E+20	-1.59	0.0
(6) H + O2(+H2) ⇆ HO2(+H2)	4.52E+13	0.0	0.0
Low	1.52E+19	-1.133	0.0
(7) H + O2(+H2O) ⇆ HO2(+H2O)	4.52E+13	0.0	0.0
Low	2.10E+23	-2.437	0.0
(8) OH + HO2 ⇆ H2O + O2	2.13E+28	-4.827	3500.0
(8b) OH + HO2 ⇆ H2O + O2	9.10E+14	0.0	10964.0
(9) H + HO2 ⇆ OH + OH	1.50E+14	0.0	1000.0
(10) H + HO2 ⇆ H2 + O2	8.45E+11	0.65	1241.0
(11) H + HO2 ⇆ O + H2O	3.01E+13	0.0	1721.0
(12) O + HO2 ⇆ O2 + OH	3.25E+13	0.0	0.0
(13) OH + OH ⇆ O + H2O	3.57E+04	2.4	-2112.0
(14) H + H + M ⇆ H2 + M	1.00E+18	-1.0	0.0
(15) H + H + H2 ⇆ H2 + H2	9.20E+16	-0.6	0.0
(16) H + H + H2O ⇆ H2 + H2O	6.00E+19	-1.25	0.0
(17) H + OH + M ⇆ H2O + M	2.21E+22	-2.0	0.0
(18) H + O + M ⇆ OH + M	4.71E+18	-1.0	0.0
(19) O + O + M ⇆ O2 + M	1.89E+13	0.0	-1788.0
(20) HO_2 + HO2 ⇆ H2O2 + O2	4.20E+14	0.0	11982.0
(20a) HO_2 + HO2 ⇆ H2O2 + O2	1.30E+11	0.0	-1629.0
(21) OH + OH(+M) ⇆ H2O2(+M)	1.24E+14	-0.37	0.0
Low	3.04E+30	-4.63	2049.0
Troe 0.470 100.0 2000.0 1.0E+15			
(22) H2O2 + H ⇆ HO2 + H2	1.98E+06	2.0	2435.0
(23) H2O2 + H ⇆ OH + H2O	3.07E+13	0.0	4217.0
(24) H2O2 + O ⇆ OH + HO2	9.55E+06	2.0	3970.0
(25) H2O2 + OH ⇆ H2O + HO2	2.40E+00	4.042	-2162.0

Table A.3: Marinov 1996 chemical kinetic model [units: s, mol, cm^3, cal and K]

Model	Third body efficiencies
Jachimowski 1988	$R_6(H_2O) = 6.0$ $R_7(H_2) = 2.0$ $R_7(H_2O) = 6.0$ $R_8(H_2O) = 5.0$ $R_9(H_2) = 2.0$ $R_9(H_2O) = 16.0$ $R_{19}(H_2O) = 15.0$
Jachimowski 1992	$\{R_6, R_7, R_8, R_9, R_10, R_{19}, R_{20}, R_{24}\} = \{H_2O = 16.0,\ H_2 = 2.5\}$
Marinov	$\{R_{17}, R_{18}\} = \{H_2O = 6.4\}$

Table A.4: Third body efficiencies for Jachimowski 1988, Jachimowski 1992 and Marinov kinetics models

References

[1] J. H. Lee, Cambridge University Press Cambridge, 2014.

[2] J. P. Tamagno, S. A. Elaskar, J. O. García, Lat. Am. Appl. Res. 42 (2) (2012) 161–166.

[3] M. H. Lefebvre, E. S. Oran, in: IUTAM Symp. Combust. Supersonic Flows, 1997, pp. 347–358.

[4] J. J. Quirk, Springer, 1994.

[5] R. Deiterding, Ph.D. thesis, Brandenburgischen Technischen Universitt Cottbus (2003).

[6] H. Jasak, A. Jemcov, Z. Tukovic, in: Int. Work. Coupled Methods Numer. Dyn., Vol. m, IUC Dubrovnik, Croatia, 2007, pp. 1–20.

[7] H. Jasak, Ph.D. thesis, PhD thesis, Imperial College, University of London. 1028 (1996).

[8] http://www.openfoam.com/ (2015).

[9] E. Robertson, V. Choudhury, S. Bhushan, D. K. Walters, Comput. Fluids 123 (2015) 122–145.

[10] B. T. Kannan, Procedia Eng. 127 (2015) 1292–1299.

[11] L. Gao, J. Xu, G. Gao, Procedia Eng. 31 (2012) 756–761.

[12] L. Orgogozo, N. Renon, C. Soulaine, F. Hénon, S. K. Tomer, D. Labat, O. S. Pokrovsky, M. Sekhar, R. Ababou, M. Quintard, Comput. Phys. Commun. 185 (12) (2014) 3358–3371.

[13] L. Orgogozo, Comput. Phys. Commun. 196 (2015) 7–8.

[14] J. Benajes, J. Galindo, P. Fajardo, R. Navarro, J. Appl. Fluid Mech. 7 (4) (2014) 673–682.

[15] A. López, W. Nicholls, M. Stickland, . W. M. Dempster, Comput. Phys. Commun. 197 (2015) 88–95.

[16] L. F. Silva, P. L. C. Lage, Comput. Chem. Eng. 35 (12) (2011) 2653–2666.

[17] G. Andreini, C. Bianchini, S. Puggelli, F. Demoulin, Int. J. Multiph. Flow 81 (2016) 88–103.

[18] P. Horgue, C. Soulaine, J. Franc, R. Guibert, G. Debenest, Comput. Phys. Commun. 187 (2015) 217–226.

[19] O. A. Marzouk, E. D. Huckaby, Eng. Lett. 18 (1) (2010) 56.

[20] L. F. Gutiérrez Marcantoni, J. P. Tamagno, S. A. Elaskar, J. Appl. Fluid Mech. 9 (2) (2016) 669–682. [link].
URL `http://jafmonline.net`

[21] H. I. Kassem, S., K. M., H. S. Aly, M. M. Sies, M. A. Wahid, Int. Commun. Heat Mass 38 (3) (2011) 363–367.

[22] S. N. P. Vegendla, D. Messig, S. Weise, C. Hasse, Energy & Fuels 25 (9) (2011) 3892–3899.

[23] J. L. Favero, A. R. Secchi, N. S. M. Cardozo, H. Jasak, J. Nonnewton. Fluid Mech. 165 (23) (2010) 1625–1636.

[24] P. Ternik, J. Nonnewton. Fluid Mech. 165 (19-20) (2010) 1400–1411.

[25] C. J. Greenshields, H. G. Weller, L. Gasparini, J. M. Reese, Int. J. for Numer. Methods in Fluids 63 (1) (2010) 1–21.

[26] B. Wüthrich, Y. Lee, in: Conf. Rec. IEEE Int. Symp. Electr. Insul., IEEE, 2008, pp. 724–727.

[27] L. F. Gutiérrez Marcantoni, J. P. Tamagno, S. A. Elaskar, in: A. Cardona, H. P. Kohan, D. R. Quinterios, M. Storti (Eds.), Mecánica Comput., Vol. 31, 2012, pp. 2939–2959.

[28] C. Shen, F. Sun, X. Xia, Comput. Phys. Commun. 185 (10) (2014) 2730–2741.

[29] O. Borm, A. Jemcov, H. P. Kau, 6th OpenFOAM Workshop, PennState University, USA, (2011).

[30] C. J. Jachimowski, Vol. 2791, National Aeronautics and Space Administration, Scientific and Technical Information Division, (1988).

[31] C. J. Jachimowski, Vol. 3224, National Aeronautics and Space Administration, Scientific and Technical Information Division, (1992).

[32] N. Marinov, C. Westbrook, W. Pitz, 8th Int. Symp. Transp. Prop. 1 (1996) 118.

[33] A. Bansal, A. Feldick, M. Modest, in: 50th AIAA Aerosp. Sci. Meeting including the New Horizons Forum and Aerospace Exposition, 2012, p. 650.

[34] V. Casseau, T. J. Scanlon, R. E. Brown, 20th AIAA Int. Sp. Planes Hypersonic Syst. Technol. Conf. (July) (2015) 1–14.

[35] V. Casseau, D. E. Espinoza, T. J. Scanlon, R. E. Brown, Aerosp. 3 (4) (2016) 45.

[36] F. Ettner, K. G. Vollmer, T. Sattelmayer, J. Combust. 2014.

[37] A. Kurganov, S. Noelle, G. Petrova, SIAM J. on Scientific Computing 23 (3) (2001) 707–740.

[38] T. Geßner, Ph.D. thesis, AlbertLudwigsUniversit at Freiburg im Breisgau (2001).

[39] N. N. Yanenko, Springer Berlin Heidelberg, Berlin, Heidelberg, 1971.

[40] G. Bader, P. Deuflhard, Number. Math 41 (3) (1983) 373–398.

[41] R. Bulirsch, J. Stoer, Numer. Math. 8 (1) (1966) 1–13.

[42] S.-T. Yu, S.-C. Chang, P. Jorgenson, S.-J. Park, M.-C. Lai, in: 36th AIAA Aerospace Sci. Meeting and Exhibit, p. 1051.

[43] K. K. Kuo., 2nd Edition, John Wiley & Sons, Inc., 2005.

[44] D. R. Stull, H. Prophet, US National Bureau of Standards, 1971.

[45] K. L. Chung, Cambridge University Press, 2010.

[46] R. Gilbert, K. Luther, J. Troe, Ber. Bunsenges. Phys. Chem. 87

598 (1983) (2006) 169–177.

[47] F. Moukalled, L. Mangani, M. Darwish, Vol. 113, Springer, 2015.

[48] I. Christov, B. Popov, J. Comput. Phys. 227 (11) (2008) 5736–5757.

[49] Y. H. Thomas, E. Tadmor, Springer-Verlag Berlin Heidelberg, 2008.

[50] B. Van Leer, J. Comput. Phys. 14 (4) (1974) 361–370.

[51] T. J. Poinsot, S. K. Lelef, J. Comput. Phys. 101 (1) (1992) 104–129.

[52] A. Cimino, G. Krause, S. Elaskar, A. Costa, Computers & Fluids 127 (2016) 194–210.

[53] L. F. Gutiérrez Marcantoni, Ph.D. thesis, Universidad Nacional de Córdoba (2016). [link].
URL https://rdu.unc.edu.ar/

[54] C. Greenshields, http://cfd.direct/openfoam/energy-equation/, online; accessed 29-December-2016 (June 2015). [link].
URL http://cfd.direct/openfoam/energy-equation/

[55] E. F. Toro, Springer Science & Business Media, 2013.

[56] C. Hirsch, Butterworth-Heinemann, 2007.

[57] R. J. Kee, F. M. Rupley, J. A. Miller, Tech. rep., Sandia National Labs., Livermore, CA (USA) (1989).

[58] R. J. Kee, M. E. Coltrin, P. Glarborg, Wiley, 2005.

[59] E. S. Oran, T. R. Young, J. P. Boris, A. Cohen, Combust. Flame 48 (C) (1982) 135–148.

[60] K.-S. Im, C. K. Kim, S. T. J. Yu, S.-C. Chang, P. C. E. Jorgenson, AIAA 1020 (2002) 2002.

[61] M. Elhsnawi, A. Teodorczyk, J. KONES 9 (1) (2002) 80–91.

[62] M. Slack, Combust. Flame 28 (1977) 241–249.

[63] G. Wilson, in: Arch. Set 484, Vol. 1, 1963.

[64] H. C. Yee, Tech. Rep. February, NASA Ames Res. Cent.; Moffett Field, CA, United States (1989).

[65] NASA (2016). [link].
URL http://www.grc.nasa.gov/WWW/CEAWeb/

[66] Y. B. Zeldovich, Z. Exsperim. Theor. Fiz 20 (1950) 175–182.

[67] J. Von Neuman (1942).

[68] W. Doring, Ann. Phys. 43 (421-436) (1943) 421–436.

[69] E. S. Oran, J. W. Weber, E. I. Stefaniw, M. H. Lefebvre, J. D. Anderson, Combust. Flame 113 (1) (1998) 147–163.

[70] R. Strehlow, A. Cohen, Phys. Fluids 5 (1) (1962) 97.

[71] D. E. Espinoza, T. J. Scanlon, R. E. Brown, in: 20th AIAA Int. Space Planes and Hypersonic Systems and Technol. Conf., 2015, pp. 35–66.

[72] S. Gottlieb, S. Chi-Wang, Math. Comput. 67 (22198) (1998) 73–85.